AGU PUBLICATIONS

JGR

Journal of Geophysical Research: Oceans

RESEARCH ARTICLE

10.1002/2015JC011231

Key Points:
- Island overwash driven by low-frequency waves and water levels on reef flat
- Extreme shoreline runup possible across a range of offshore conditions
- Sea level rise leads to increased overwash and runup on fringing reef coasts

Correspondence to:
O. M. Cheriton,
ocheriton@usgs.gov

Citation:
Cheriton, O. M., C. D. Storlazzi, and K. J. Rosenberger (2016), Observations of wave transformation over a fringing coral reef and the importance of low-frequency waves and offshore water levels to runup, overwash, and coastal flooding, *J. Geophys. Res. Oceans*, *121*, 3121–3140, doi:10.1002/2015JC011231.

Received 12 AUG 2015
Accepted 12 APR 2016
Accepted article online 19 APR 2016
Published online 13 MAY 2016

Observations of wave transformation over a fringing coral reef and the importance of low-frequency waves and offshore water levels to runup, overwash, and coastal flooding

Olivia M. Cheriton[1], Curt D. Storlazzi[1], and Kurt J. Rosenberger[1]

[1]Pacific Coastal and Marine Science Center, U.S. Geological Survey, Santa Cruz, California, USA

Abstract Many low-lying tropical islands are susceptible to sea level rise and often subjected to overwash and flooding during large wave events. To quantify wave dynamics and wave-driven water levels on fringing coral reefs, a 5 month deployment of wave gauges and a current meter was conducted across two shore-normal transects on Roi-Namur Island in the Republic of the Marshall Islands. These observations captured two large wave events that had waves with maximum heights greater than 6 m with peak periods of 16 s over the fore reef. The larger event coincided with a peak spring tide, leading to energetic, highly skewed infragravity (0.04–0.004 Hz) and very low frequency (0.004–0.001 Hz) waves at the shoreline, which reached heights of 1.0 and 0.7 m, respectively. Water surface elevations, combined with wave runup, reached 3.7 m above the reef bed at the innermost reef flat adjacent to the toe of the beach, resulting in flooding of inland areas. This overwash occurred during a 3 h time window that coincided with high tide and maximum low-frequency reef flat wave heights. The relatively low-relief characteristics of this narrow reef flat may further drive shoreline amplification of low-frequency waves due to resonance modes. These results (1) demonstrate how the coupling of high offshore water levels with low-frequency reef flat wave energetics can lead to large impacts along fringing reef-lined shorelines, such as island overwash, and (2) lend support to the hypothesis that predicted higher sea levels will lead to more frequent occurrences of these extreme events, negatively impacting coastal resources and infrastructure.

1. Introduction

Coral reefs that surround low-lying islands and land masses provide important protection against the impact of large waves and storm damage [*Ferrario et al*., 2014], including tsunamis [*Kunkel et al*., 2006], by energy dissipation through wave breaking and bottom friction [*Lowe et al*., 2005]. However, climate change and sea level rise have led to growing concern for how the hydrodynamics across these reefs will evolve and whether these changes will leave islands more vulnerable to large wave events [*Storlazzi et al*., 2011; *Grady et al*., 2013; *Merrifield et al*., 2014; *Storlazzi et al*., 2015a].

Because the majority of reef flats are depth limited, with many going dry during lower low tides, offshore water levels (i.e., tidal stage) strongly control the ability of waves to propagate across a reef and impact the shoreline [e.g., *Young*, 1989; *Brander et al*., 2004; *Hoeke et al*., 2013]. In addition to offshore water levels, wave-induced setup also contributes to reef flat water levels; as offshore swell breaks over the shallow reef topography, the change in radiation stress leads to a water level increase ("setup") over the reef flat [*Longuet-Higgins and Stewart*, 1964]. Setup is strongly governed by offshore wave height and period [*Hench et al*., 2008], but is also dependent on tidal stage in that setup generally increases with decreasing water levels on the reef [*Seelig*, 1983; *Vetter et al*., 2010; *Becker et al*., 2014], so the potential effects of wave-induced setup are greatest at low tide phases.

Due to the complex bathymetry and wave dynamics characteristic of reef environments, the transformation of waves over reefs is distinctly different from that on sandy beaches [*Lee and Black*, 1978]. Waves propagating onto shallow reefs steepen and break, and while some of the breaking wave energy propagates shoreward as reformed high-frequency ($0.04 < f < 0.2$ Hz, i.e., "incident") waves, the spectral wave energy shifts into lower frequencies and long-period ($f < 0.04$ Hz; i.e., "infragravity") waves often dominate. Observations of how low-frequency waves become increasingly important across reef flats (from the reef crest toward shore) have been reported for a variety of environments [e.g., *Hardy and Young*, 1996; *Lugo-Fernandez et al*.,

1998; *Péquignet et al*., 2011; *A. Pomeroy et al*., 2012a; *Ford et al*., 2013; *Beetham et al*., 2015] and have also been demonstrated in laboratory and modeling studies [*Nwogu and Demirbilek*, 2010; *Torres-Freyermuth et al*., 2012; *van Dongeren et al*., 2013; *Shimozono et al*., 2015]. These low-frequency waves are thought to be generated in the surf zone by breakpoint forcing [*A. Pomeroy et al*., 2012a], where the time-varying oscillation of the shore wave breakpoint produces free low-frequency waves [*Symonds et al*., 1982]. This stands in contrast to the bound low-frequency waves that form via the nonlinear interactions between short-period wind/gravity waves shoaling over gently sloping seabeds [*Longuet-Higgins and Stewart*, 1960].

Previous observations of low-frequency waves over shallow reef flats have established relationships between the offshore conditions and resulting reef flat wave characteristics. Over depth-limited reef flats, short-period wave heights are primarily governed by water levels [*Hardy and Young*, 1996; *A. Pomeroy et al*., 2012a; *Becker et al*., 2014]. Low-frequency wave heights are also controlled by water levels but equally influenced by the offshore incident wave heights and periods, in that greater offshore wave power impinging on the reef crest leads to larger low-frequency waves over the reef flat [*A. Pomeroy et al*., 2012a]; this is due in part to the increased water levels generated by wave-induced setup [*Péquignet et al*., 2011].

The importance of low-frequency waves to reef flat water level dynamics has recently been explored by a number of field [*A. Pomeroy et al*., 2012a; *Ford et al*., 2013; *Péquignet et al*., 2014; *Beetham et al*., 2015] and laboratory and modeling studies [*Nwogu and Demirbilek*, 2010; *Torres-Freyermuth et al*., 2012; *van Dongeren et al*., 2013; *Pomeroy et al*., 2015]. There is increasing evidence that low-frequency waves not only tend to dominate the nearshore reef flat wave patterns, but may also be the significant forcing behind many coastal hazard processes, such as shoreline accretion/erosion, wave overwash, flooding, and beach runup. *Hardy and Young* [1996] noted the nonlinear shape ("sharp peaks and long flat troughs") of waves propagating across a reef flat. This skewness and asymmetry of low-frequency waves likely contributes to cross-shore transport of sediment and other material, as was demonstrated in a recent laboratory experiment by *Pomeroy et al*. [2015]. During large storms and wave events, this transport may be a key determinant of subsequent shoreline erosion or accretion, as has been observed for planar beach coastlines [*Aagaard and Greenwood*, 1995].

Additionally, during large wave events, low-frequency waves may have a disproportionately large impact by driving resonance [*Péquignet et al*., 2009], runup [*Merrifield et al*., 2014; *Shimozono et al*., 2015], and overwash [*Hoeke et al*., 2013]. *Seelig* [1983] defined runup as the maximum wave-driven vertical uprush elevation (above the mean water level) that occurs on land. The early laboratory study by *Seelig* [1983] noted how runup was strongly influenced by offshore "surf beat" and increased under irregular wave forcing at the simulated reef crest. These observations pointed to the role of low-frequency waves in generating runup, however, only recently have the processes governing runup on fringing reef-lined coasts been more thoroughly investigated. In their laboratory experiments and numerical simulations, *Nwogu and Demirbilek* [2010] identified the importance of low-frequency waves to resultant runup, and found that reef flat resonance can further increase runup at the shoreline. Several recent modeling studies also report that shoreline runup is dominated by contributions from the low-frequency ($<$0.04 Hz) band [*Beetham et al*., 2015; *Shimozono et al*., 2015]. Under intense storm conditions, the amplification of runup by reef flat resonance patterns can lead to extreme coastal inundation and flooding: when super typhoon Haiyan made landfall in the central Philippines, the interaction between shoreline resonance and the incident and infragravity waves on the reef flat drove runup that exceeded 10 m [*Shimozono et al*., 2015]. In addition, modeling work by *Quataert et al*. [2015] was the first to demonstrate how reef characteristics influence resultant runup, with the greatest runup associated with narrow, relatively smooth (low-friction) reefs; they also found that rising sea levels cause an increase in runup—findings that have since been replicated by other models [*Beetham et al*., 2015; *Shimozono et al*., 2015]. Using a model based on field observations from a narrow reef on Funafuti Atoll, Tuvalu, *Beetham et al*. [2015] showed how a fringing reef-lined beach can be affected by runup a majority of the time, even if the connecting reef flat is exposed during low tides. This frequency of exposure to runup is also predicted to increase with sea level rise [*Beetham et al*., 2015].

These laboratory and model-based studies provide projections of reef flat hydrodynamics under large wave forcing and suggest that low-frequency motions are the primary drivers of resulting extreme shoreline processes such as overwash and large runup. However, direct field observations of reef wave dynamics during storm events are limited. They include reports on the impact of Typhoon Russ [*Jaffe and Richmond*, 1992] and Typhoon Man-Yi [*Péquignet et al*., 2009; *Vetter et al*., 2010] on fringing reefs in Guam, as well as a small overwash event on Majuro Atoll, Republic of the Marshall Islands (RMI) [*Ford et al*., 2013]. Here we present

direct in situ and shoreline-based observations of two large (1–2 occurrences per year; based on mean wave characteristics for 2 year scenario model hindcast [*Storlazzi et al*., 2015b]) wave events on the fringing reef of Roi-Namur Island, RMI, that resulted in overtopping of shoreline berms (overwash) and flooding of inland areas. We also assess the nonlinear characteristics of these low-frequency waves, and demonstrate how they drive runup patterns at the shoreline during both storm and nonstorm conditions. Our results demonstrate how the coupling of high water levels with low-frequency reef flat wave energetics can lead to large impacts at the shoreline, such as runup and overwash, and lend support to the hypothesis that higher sea levels will lead to more frequent occurrences of these extreme events.

The findings herein are organized as follows: section 3.1 describes the general wave patterns across the reef flat, including the cross-reef wave energy, nonlinearity, skewness, and asymmetry. Section 3.2 presents the observations from the two large wave events. Then, section 3.3 explores a large "anomalous" runup event that did not occur during either of the large wave events. Following these results, we discuss the role of reef morphology and low-frequency wave propagation, focusing on the role of frictional dissipation (section 4.1). And, given the morphology and frictional characteristics of the reef, we explore the possibility of low-frequency wave resonance over the reef flat (section 4.2). Then, we discuss how low-frequency waves can have a disproportionate impact at shorelines through both accretion/erosion effects (section 4.3), as well as runup (section 4.4). We conclude with a discussion of how these findings inform predictions regarding coastal hazards for fringing reef-lined coasts given future climate change (section 4.5).

2. Methods

2.1. Study Area

The experiment took place in the Republic of the Marshall Islands (RMI), a Pacific island nation that is located roughly halfway between Hawaii and Australia and is composed of 29 low-lying coral atolls and 5 single coral islands. Kwajalein Atoll, RMI, has a mean island elevation of 1.8 m and is considered the second largest atoll in the Pacific Ocean, encompassing an area of over 2000 km^2 [*U.S. Department of Interior*, 2006]. The study site was located on the island of Roi-Namur at the northern point of Kwajalein Atoll (Figure 1a). Because of its orientation, the northern (ocean-side) coastline is primarily subjected to northerly swell and northeast trade wind waves.

The fringing reef at the study site is characterized by a gently sloping (∼1:110) platform that ranges from 250 to 350 m wide, is relatively smooth, and predominantly covered by coralline algae (Figure 1). The reef flat has an average depth of 0.7 m, is mostly exposed at lower low tide, and extends from a narrow, steep (∼1:6), 3–4 m high sandy beach to a slightly elevated reef crest. Offshore of the reef crest, the fore reef slope is steep (∼1:20; Figures 1b and 1c) and is characterized by high coral cover and relief.

2.2. Wave Measurements

From 3 November 2013 to 13 April 2014, we deployed two cross-shore transects ("NW" and "NE") of bottom-mounted RBR virtuoso wave gauges (i.e., pressure sensors) over the reef flat and fore reef (Figure 1). Each transect consisted of three gauges on the reef flat and one gauge on the upper fore reef at depths ∼7 m. The NE1 fore reef record is not included due to sensor failure. The two transects were 650–800 m apart, and between them an upward-looking 600 kHz Nortek Acoustic Wave and Current Meter (AWAC) was placed deeper on the fore reef (∼21 m depth). Every hour the wave gauges collected pressure measurements at 2 Hz in 34 min bursts (4096 samples) and the AWAC recorded pressure at 1 Hz in 34 min bursts (2048 samples). For the analyses presented herein, the pressure bursts from the AWAC were used to allow direct comparison with the wave gauge records. The wave parameters obtained from the dynamic acoustic surface-tracking feature of the AWAC were used to verify those computed from the pressure records and to determine maximum recorded wave heights, H_{max}. To distinguish between the fore reef sensors, the AWAC site (N0) is referred to as "offshore," while the NW1 wave gauge site is referred to as "fore reef."

The following method for calculating bulk wave statistics was applied across all pressure sensors. Atmospheric pressure measurements from the Kwajalein airport weather station were obtained through the National Oceanic and Atmospheric Administration's National Climate Data Center (gis.ncdc.noaa.gov), and these interpolated records were subtracted from each pressure burst. The resultant sea pressure values were converted to water levels. Note: herein we will use h to refer to the burst-mean water level, while h'

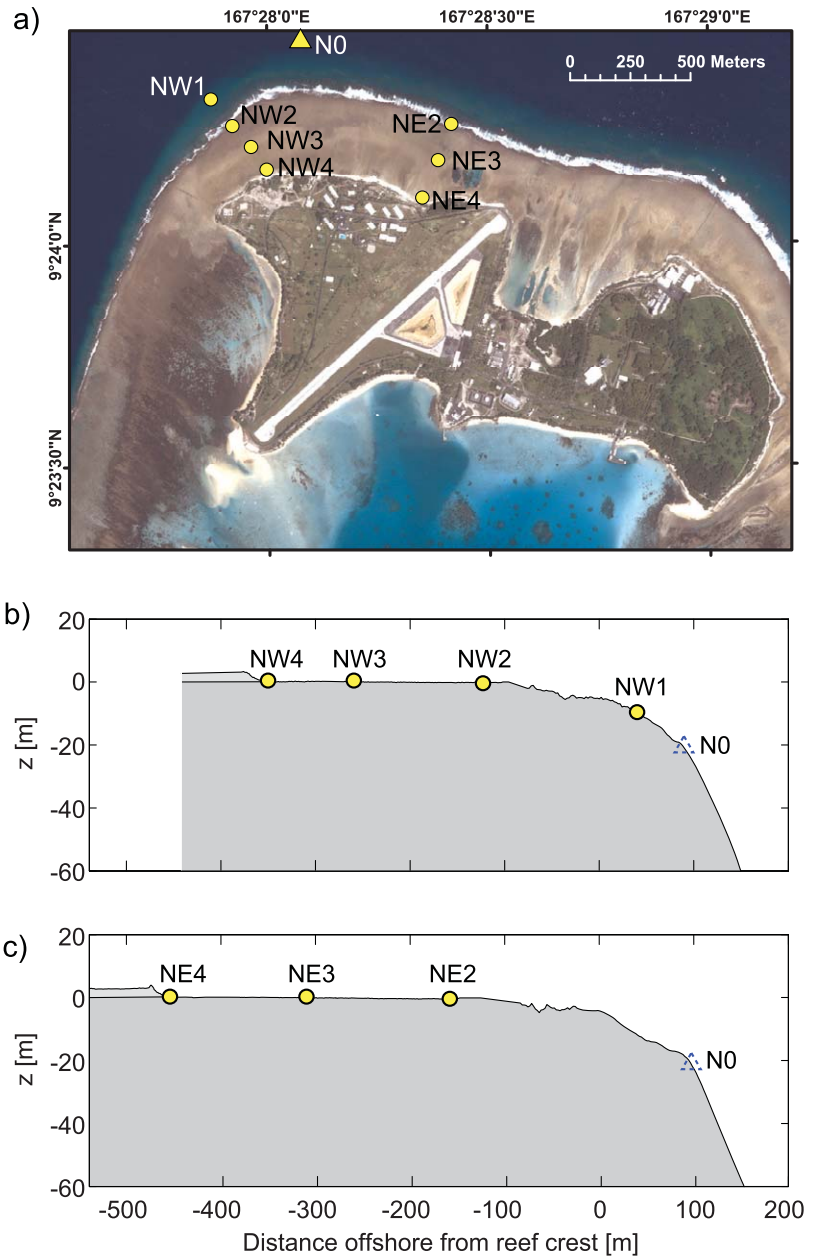

Figure 1. Map of Roi-Namur Island (a) showing locations of instruments in cross-reef arrays including wave gauges (yellow circles) and the offshore AWAC (yellow triangle). Cross-reef profiles for (b) NW and (c) NE transects showing reef bathymetry and relative cross-reef distances between wave gauges (yellow circles) according to distance from the reef crest. The depth of the AWAC ("N0") relative to the wave gauges is indicated on these profiles, however, because it was not along a shore-normal transect line to the wave gauges, the cross-reef distance is not accurate.

indicates the instantaneous water level measured within a burst, and h'_{max} is the maximum h' within a given burst. The one-dimensional energy spectra, $S(f)$, were computed using the Welch's averaged modified periodogram method, which utilizes a Hamming window (length of 2048 elements ~17 min) with 50% overlap. Pressure response factor corrections were applied to the spectra. The $S(f)$ records were then partitioned along frequency bands chosen for incident ("IC"; 0.20–0.04 Hz), infragravity ("IG"; 0.040–0.004 Hz), and very low frequency ("VLF"; 0.004–0.001 Hz) waves. The purpose of separating the low-frequency band into the IG and VLF partitions was to illustrate the importance of the VLF wave energy for our reef flat observations. However, we note that there is both no natural frequency separation between these two bands, as often exists between the short-period and long-period wave energy, and that the resolution obtained in the VLF band is limited (see Figure 2).

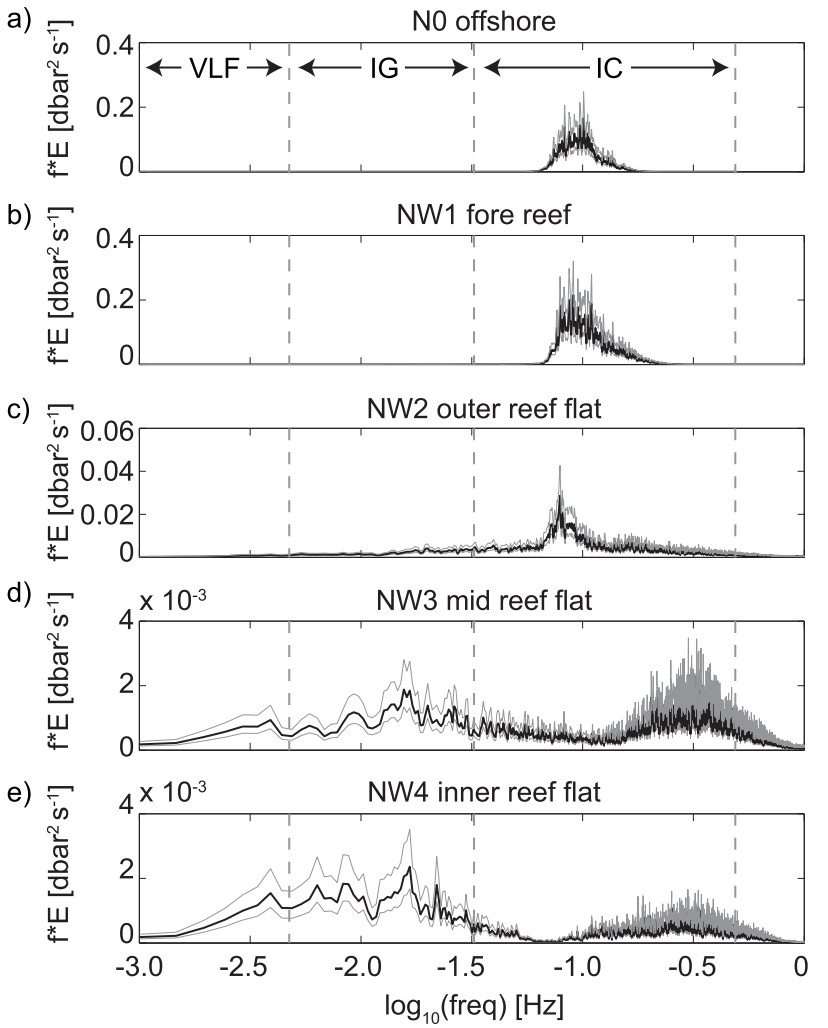

Figure 2. Variance-preserving energy spectra from a representative burst during the March large wave event, showing the transfer of energy to lower frequencies that occurs from the outer to inner reef flat. The gray lines indicate the 95% confidence interval. The regions of the incident (IC), infragravity (IG), and very low frequency (VLF) bands are denoted by the vertical dashed lines.

Significant wave height, H_s, was determined as

$$H_s = 4\sqrt{\int_{f_1}^{f_2} S(f)df} \tag{1}$$

And the root-mean-squared wave height, H_{rms}, was computed as

$$H_{rms} = \sqrt{8\int_{f_1}^{f_2} S(f)df} \tag{2}$$

where, for both (1) and (2), f_1 and f_2 are the lower and upper frequency limits for each wave band. The peak period, T_p, was identified as the frequency associated with the peak energy in each band, and the total energy associated with each frequency band was determined as $E=(1/2)(H_{rms}/2)^2$. Because the majority of the reef flat was exposed at low tides, all analyses using reef flat wave parameters only include times when inner reef flat water levels were at least 0.2 m.

Wave-induced setup over the reef flat, η, was calculated after *Vetter et al.* [2010] as $\eta = h - h_{off} - (bt + c)$, where h and h_{off} are the burst-averaged water levels at the reef flat and offshore, respectively, and b and c are best fit parameters to account for relative pressure drift between the two sensors over time. Then,

following *Becker et al.* [2014], the resulting η was normalized to the computed setdown at the offshore site, η_{off}, determined by the *Longuet-Higgins and Stewart* [1962] formula:

$$\eta_{off} = -\frac{H_{rms,off}^2 k_{off}}{8\sinh(2k_{off}h_{off})} \tag{3}$$

in which $H_{rms,off}$ is the offshore root-mean-squared offshore wave height, and k_{off} is the offshore wave number. We note that η_{off} was never lower than -0.02 m. And, while η_{off} referenced to this site may not necessarily equal the maximum setdown offshore of the reef crest, we consider it a valid estimate, as setdown at the fore reef site (NW1) was also $O(-0.01)$ m.

Three parameters were used to assess the characteristics of the observed waves: the Ursell number, wave skewness, and wave asymmetry. The Ursell number [*Ursell*, 1953] is a dimensionless parameter often used to quantify the nonlinearity of surface waves [e.g., *Kirby and Dalrymple*, 1984; *Osborne et al.*, 1996; *Peng et al.*, 2009]. The local Ursell number, U, utilizes the horizontal and vertical extents of a wave (relative to water depth) and is defined as

$$U = \frac{H_s \lambda^2}{h^3} \tag{4}$$

where the wavelength, λ, was determined from the wave period. Wave skewness and asymmetry were estimated under the assumption that the reef flat waves can be considered long waves, with the wave orbital velocities proportional to the free surface elevation [e.g., *Dean and Dalrymple*, 1991]. Wave skewness, Sk, and asymmetry, As, were calculated using the third-order moments of h [*Grasso et al.*, 2011; *Pomeroy et al.*, 2015],

$$Sk = \frac{\langle \tilde{h}^3 \rangle}{\langle \tilde{h}^2 \rangle^{3/2}} \tag{5}$$

$$As = \frac{\left\langle \mathcal{H}^3\left(\tilde{h}\right) \right\rangle}{\langle \tilde{h}^2 \rangle^{3/2}} \tag{6}$$

where $\mathcal{H}$ is the Hilbert transform and the "$\sim$" indicates the deviation from the burst mean.

3. Results

3.1. Wave Patterns Across the Reef Flat

Wind patterns throughout the study were dominated by northeasterly trade winds, and tides were predominantly semidiurnal, with a range of approximately ± 1 m (Figure 3). Offshore significant wave heights averaged 1.6 m at 10.9 s, with an H_s range of 0.7 to 4.0 m, and a T_p range of 5.0–18.3 s. H_{max} averaged 2.9 m, with peak wave heights reaching 6.9 m. Waves were predominantly out of the northwest to northeast, with a mean direction of 19°T and a range of -33 to 50°T (Figure 3e). The contribution to the overall sea state by locally wind-forced waves was small compared to the remotely generated swell. While IC waves dominated over the fore reef, $H_{s,IG}$ and $H_{s,VLF}$ often grew larger than $H_{s,IC}$ by the mid to inner reef flat. For both transects, the largest reef flat $H_{s,IC}$ was observed at the outer reef flat sites, and decayed shoreward. Reef flat $H_{s,IG}$ and $H_{s,VLF}$ increased toward shore, with the greatest wave heights at the innermost reef flat sites. Across both reef flat transects, $H_{s,IG}$ averaged 0.2 m, with peak values reaching nearly 1.0 m. The average $H_{s,VLF}$ was 0.1 m, but could reach heights of 0.7 m. Over the depth-limited reef flat, $H_{s,IC}$ increased and decreased according to water levels. Water levels also influenced the reef flat $H_{s,IG}$ and $H_{s,VLF}$, but low-frequency wave heights were also controlled by the offshore incident wave heights and periods, in that greater offshore wave power on the fore reef led to larger low-frequency waves over the reef flat. These findings are in agreement with previous observations [*Hardy and Young*, 1996; *Péquignet et al.*, 2011; *A. Pomeroy et al.*, 2012a; *Becker et al.*, 2014; *Beetham et al.*, 2015]. We also explored the role of offshore wave groupiness [*List*, 1991] on the observed reef flat wave dynamics, but found no significant correlations between the groupiness factor of offshore waves and resulting reef flat wave characteristics.

We examined the cross-reef patterns of wave energy, E, as well as the waveform characteristics through the Ursell number, U, wave skewness, Sk, and wave asymmetry, As. The energy and nonlinearity of reef flat

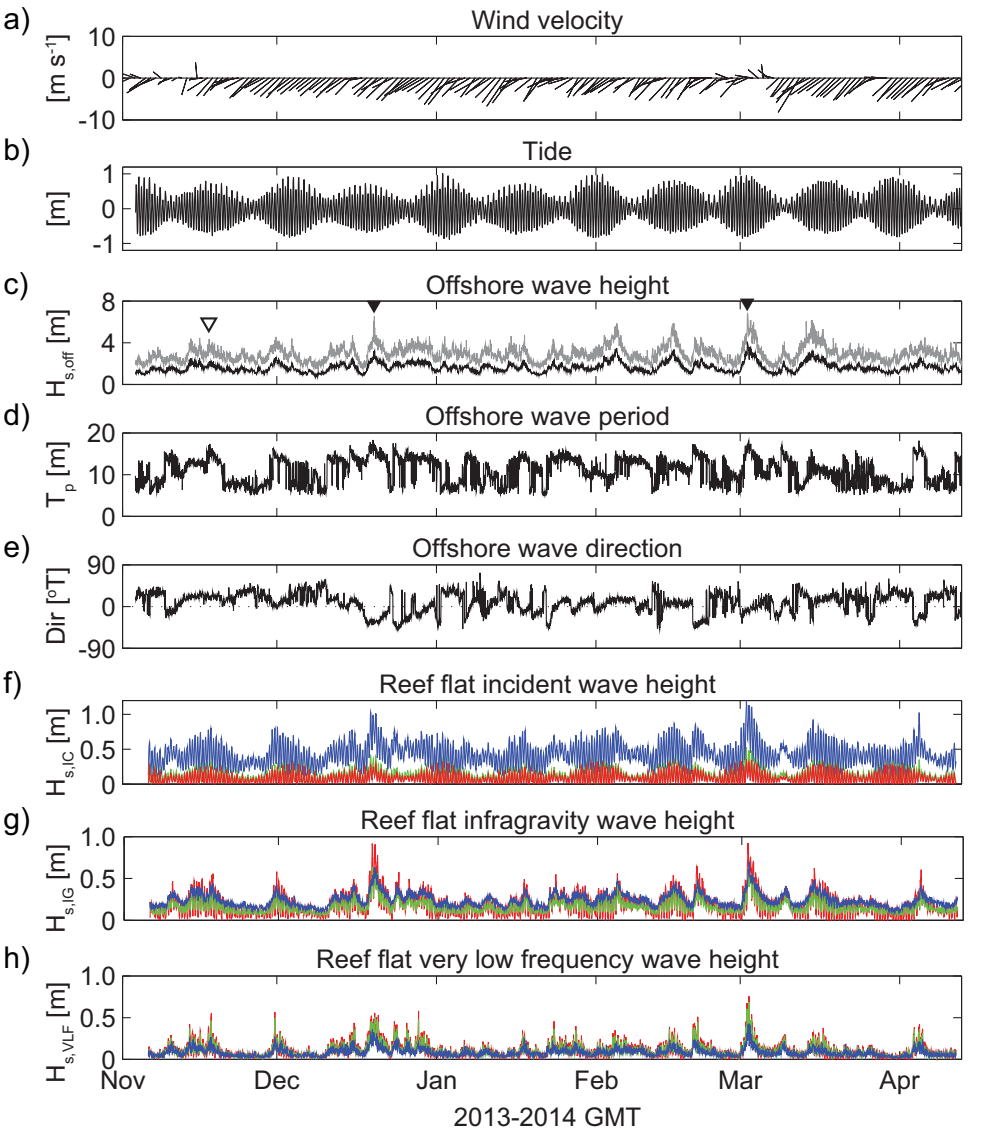

Figure 3. Time series of meteorologic and oceanographic conditions during the 5 month deployment. (a) Daily-averaged wind velocity, with stick vectors indicating heading; (b) offshore tide levels; (c) offshore significant (black) and maximum (gray) wave heights, with black triangles indicating the two large wave events and the open triangle indicating the 18 November runup event; (d) offshore wave period; (e) offshore wave direction from true north. (f) Incident, (g) infragravity, and (h) very low frequency reef flat wave heights for the outer (blue), mid (green), and inner (red) NW reef flat sites.

waves varied in response to a range of water levels and offshore wave conditions. From the outer to inner reef flat, E_{IC} decreased while E_{IG} and E_{VLF} showed little loss across the reef flat (Figures 4a, 4e, and 4i), particularly under average to high water levels, suggesting minimal frictional dissipation over the reef flat for these low-frequency waves. The cross-reef low-frequency wave energy also exhibited standing mode patterns during higher reef flat water levels and the large wave events; E_{IG} peaked at the outer and inner reef flat, with a node near the mid-reef site, while E_{VLF} increased from a minimum at the outer reef flat to maximum at the inner site, possibly indicative of the fundamental mode. Under mean or lower-than-average reef flat water levels, these resonance patterns were not evident and the low-frequency wave energy at the inner reef flat was markedly decreased, likely due to the increased importance of frictional dissipation with decreased water levels.

Across all wave types, nonlinearity was controlled by reef flat water levels, with increasing nonlinearity with lower water levels (Figures 4b, 4f, and 4j). The incident wave nonlinearity, U_{IC}, consistently peaked at the outer reef flat site, while U_{IG} and U_{VLF} increased across the reef flats toward shore, peaking at the innermost

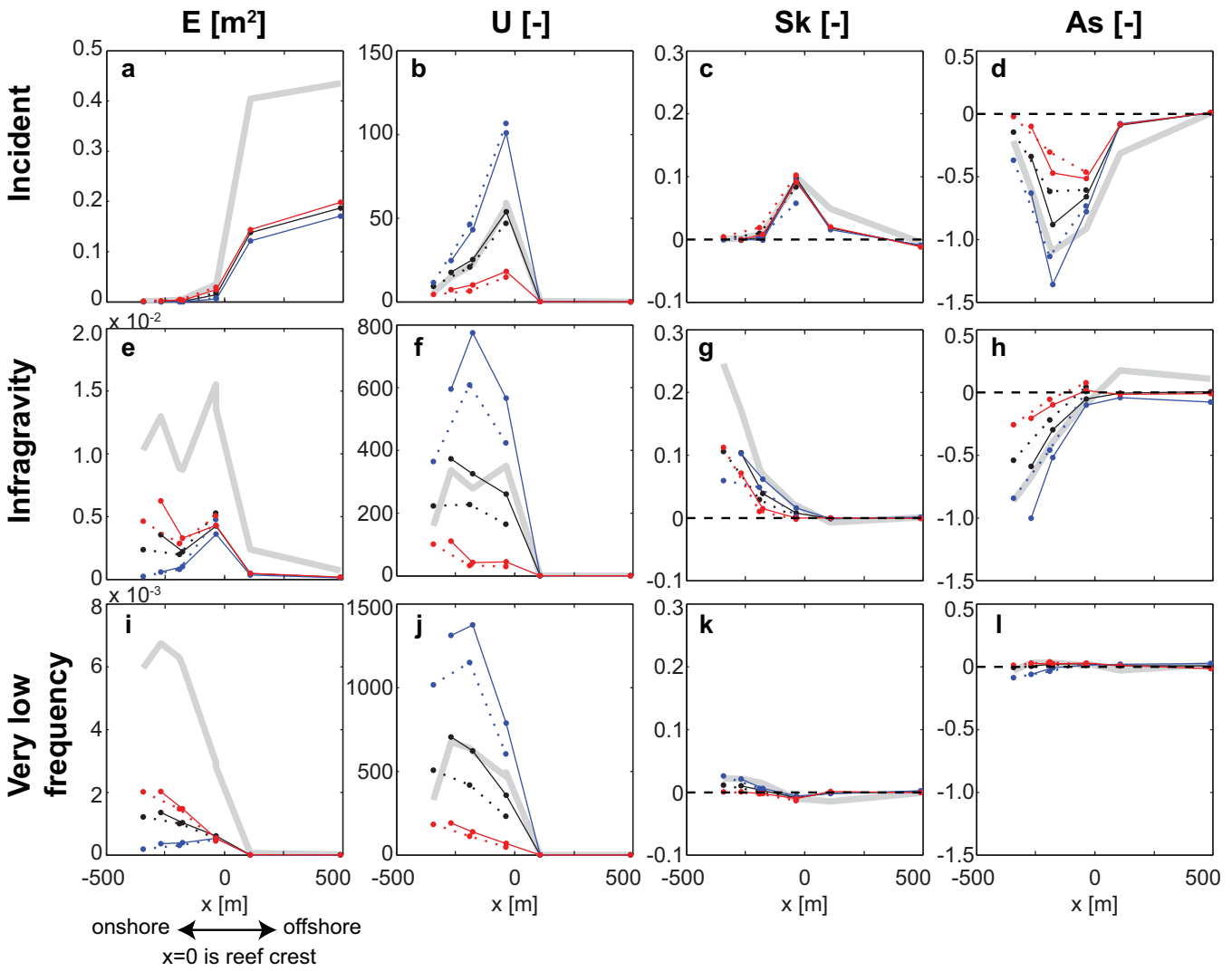

Figure 4. Cross-reef average values of wave characteristics for (a–d) incident (IC), (e–h) infragravity (IG), and (i–l) very low frequency (VLF) waves according to distance offshore of reef crest. For all plots, average profiles for overall (black), low water levels (blue), high water levels (red), and the two large wave events (thick gray) are shown for both the NW (solid line) and NE (dotted line) transects. The most offshore data point is the N0 site. (a, e, and i) Wave energy, *E*; (b, f, and j) Ursell number, *U*; (c, g, and k) wave skewness, *Sk*; (d, h, and l) wave asymmetry, *As*. Note that *y* axis limits for the first and second columns vary.

reef flat sites under high or average water levels. During times of low water levels, peak low-frequency wave nonlinearity was reached closer to mid-reef, probably due to depth limitations at the inner reef sites. The general pattern of wave skewness showed Sk_{IC} maximum at the outer reef flat sites, consistent with short-period wave breaking at the reef crest (Figure 4c). From the outer to inner reef flat, Sk_{IG} increased and was particularly enhanced during the large wave events (Figure 4g). The Sk_{VLF} remained near zero across all sites and water levels (Figure 4k). Wave asymmetry was sensitive to water levels, with lower water levels leading to greater *As* magnitudes for IC and IG waves (Figures 4d and 4h). As_{IC} magnitudes were largest at mid-reef flat sites, while As_{IG} increased toward shore, with maximum (negative) asymmetry at the inner reef flat sites, particularly under low water levels or large offshore wave conditions. The negative asymmetry indicates that these waves are pitched forward, with steep front faces and more gently sloping rear faces. These skewed and asymmetric IG waves may disproportionally drive cross-shore transport of reef material during high energy events [*Malarkey and Davies*, 2012; *Terry et al.*, 2013; *Pomeroy et al.*, 2015].

Despite the positive skewness and negative asymmetry associated with the IG reef flat waves, it is unlikely that these waves were breaking at the inner reef flat, given the steep slope of the beach (1:6). With the suite of instruments used, it is not possible to distinguish between shoreward and seaward propagating reef flat waves. However, to evaluate whether these waves were in a reflective or breaking regime, we can utilize

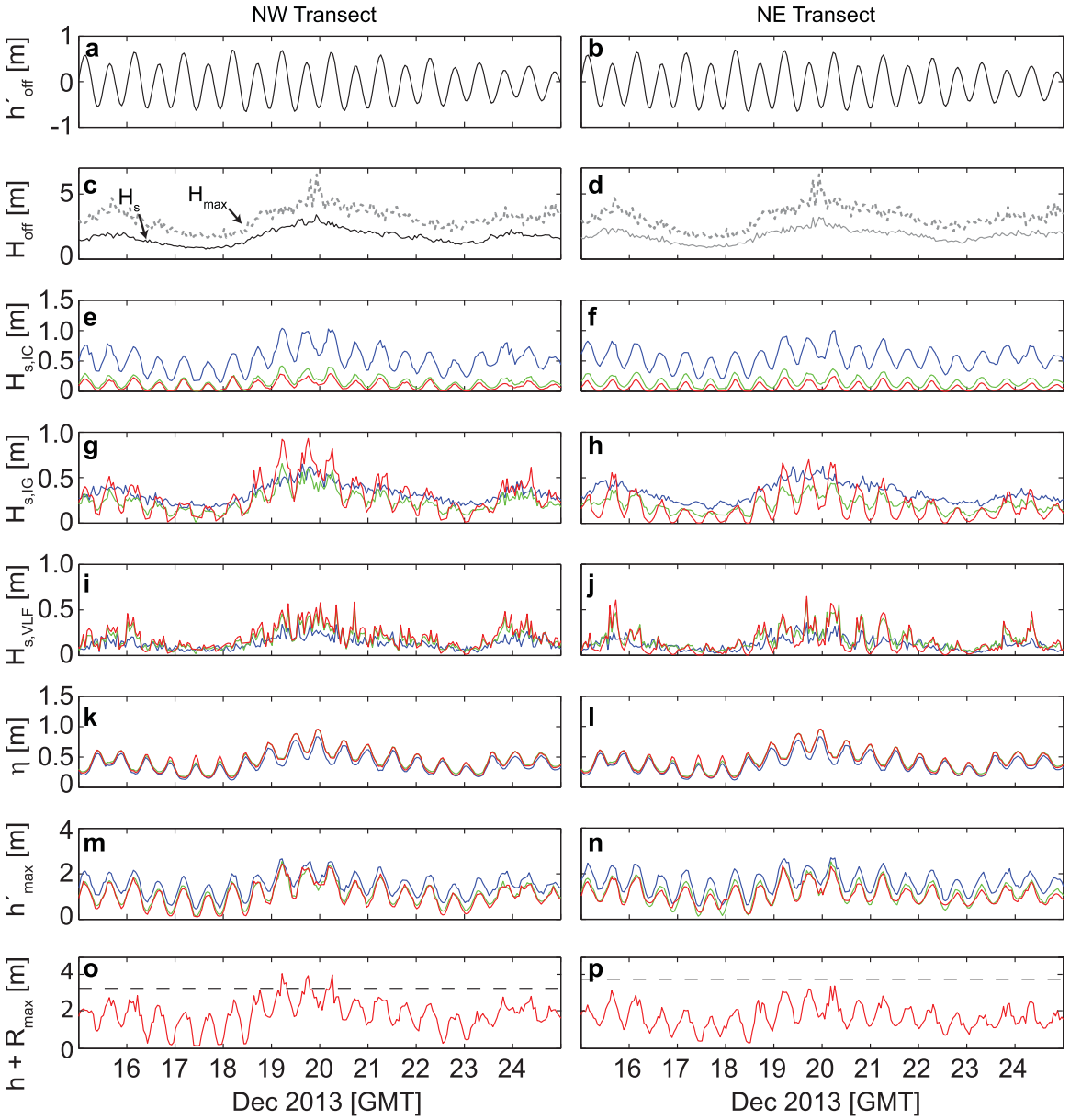

Figure 5. Time series of 10 day period covering the December 2013 large wave event for both the (left column) NW and (right column) NE transects. (a, b) Water levels from the mean from the offshore site; (c, d) offshore maximum wave heights (gray dotted) and fore reef significant wave heights (black solid); in Figure 5d, significant wave heights from offshore site (gray solid) due to no fore reef data. For subsequent (third through eighth) rows, measurements from outer (blue), mid (green), and inner (red) reef flat sites: (e, f) incident wave heights; (g, h) infragravity wave heights; (i, j) very low frequency wave heights; (k, l) setup; (m, n) maximum instantaneous water levels for each burst; (o, p) burst-averaged water levels plus total (incident + infragravity) maximum runup estimates, with the black dashed line indicating the vertical height of the beach berm at the inner reef flat site.

the reflection coefficient found by *Battjes* [1974] and validated for low-frequency waves by *van Dongeren et al.* [2007]: $R=0.2\pi\beta_H$. Here β_H is essentially a normalized bed slope that is proportional to the Iribarren number (or surf similarity parameter) and is given by $\beta_H=\beta T/\left(2\pi\sqrt{g/H}\right)$, where β is the bed slope, H is the low-frequency wave height with associated period T, and g is the gravitational acceleration (9.81 m s^{-2}) [*de Bakker et al.*, 2014]. The resulting R for the observed IG and VLF reef flat waves indicates a fully reflective regime, with $R \gg 1$ through the study period.

3.2. Large Offshore Wave Events and Overwash

Two large wave events, with $H_{max} > 6$ m and $T_p > 15$ s, impacted Roi-Namur during this experiment: (1) 19 December 2013 ("December event"; Figure 5) and (2) 2–3 March 2014 ("March event"; Figure 6). Model hindcasts for this area estimate wave events of this magnitude impacting the Kwajalein Atoll roughly every 2

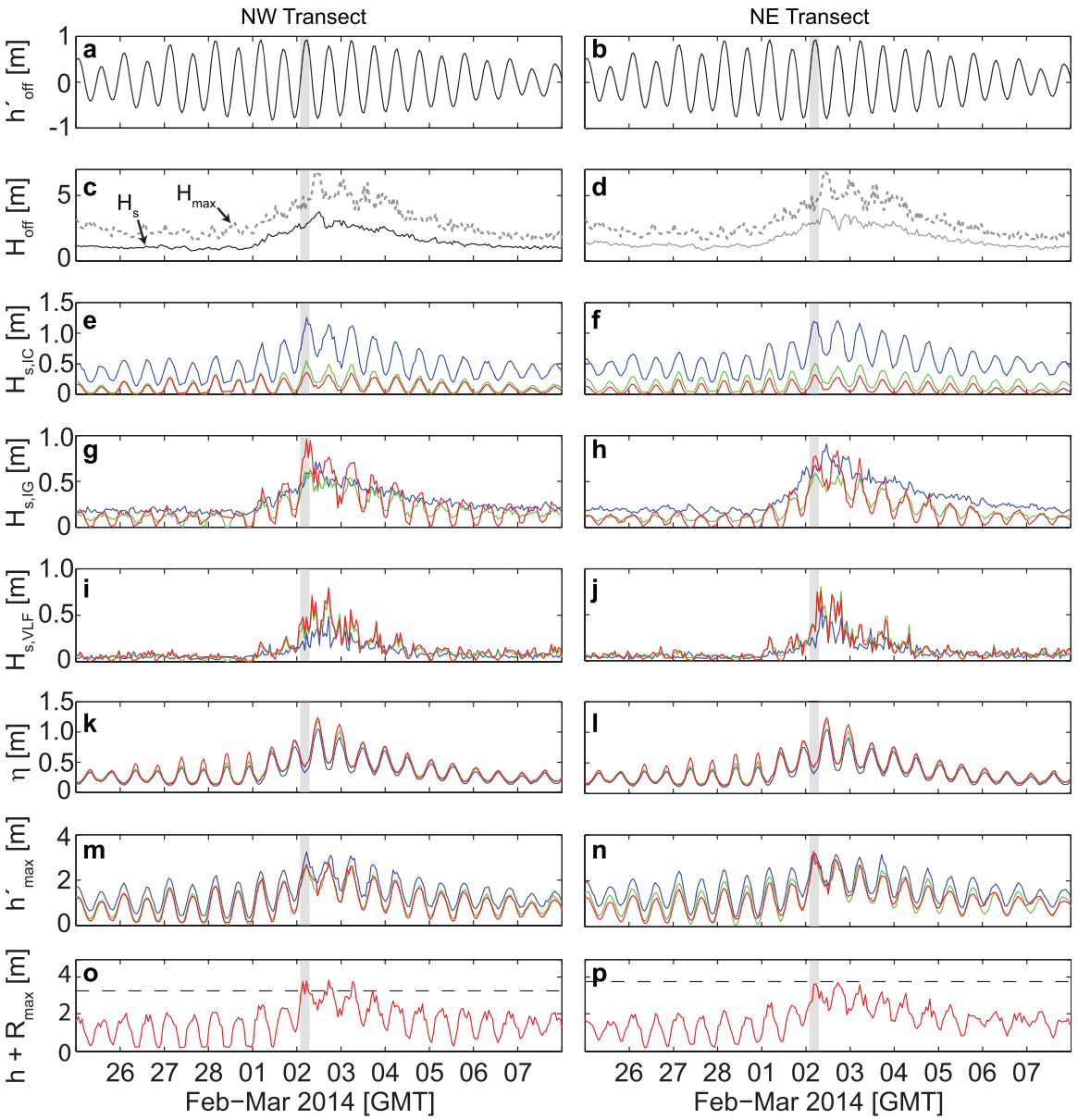

Figure 6. Time series of 10 day period covering the March 2014 large wave event for both the (left column) NW and (right column) NE transects. (a, b) Water levels from the mean from the offshore site; (c, d) offshore maximum wave heights (gray dotted) and fore reef significant wave heights (black solid); in Figure 6d, significant wave heights from offshore site (gray solid) due to no fore reef data. For subsequent (third through eighth) rows, measurements from outer (blue), mid (green), and inner (red) reef flat sites: (e, f) incident wave heights; (g, h) infragravity wave heights; (i, j) very low frequency wave heights; (k, l) setup; (m, n) maximum instantaneous water levels for each burst; (o, p) burst-averaged water levels plus total (incident + infragravity) maximum runup estimates, with the black dashed line indicating the vertical height of the beach berm at the inner reef flat site. The gray shaded box in each plot indicates the period of eye-witnessed overwash (P. Swarzenski, personal communication).

years [*Storlazzi et al.*, 2015b]. During both events, $H_{s,IC}$ at the outer reef flat of both transects exceeded 1 m, while $H_{s,IG}$ at the inner reef flat site adjacent to the beach reached approximately 1 m. Reef flat $H_{s,VLF}$ and water level setup η were greater during the March event than the December event; during the March event, $H_{s,VLF}$ reached 0.7 m at the mid to inner reef flat, and at low tide $\eta > 1$ m. Offshore conditions during the March event differed from those during the December event, primarily in terms of incoming wave direction and tidal stage. During the December event, peak swell was out of the north-northeast (−33°T), approximately −5°(−52°) from shore-normal for the NW(NE) reef flat, whereas during the March event, the swell was almost directly out of the north (−4°T), corresponding to 24°(−23°) from shore-normal for the NW(NE) transects. The December event occurred during the transition from spring to neap tide, whereas the March event occurred at the height of spring tide.

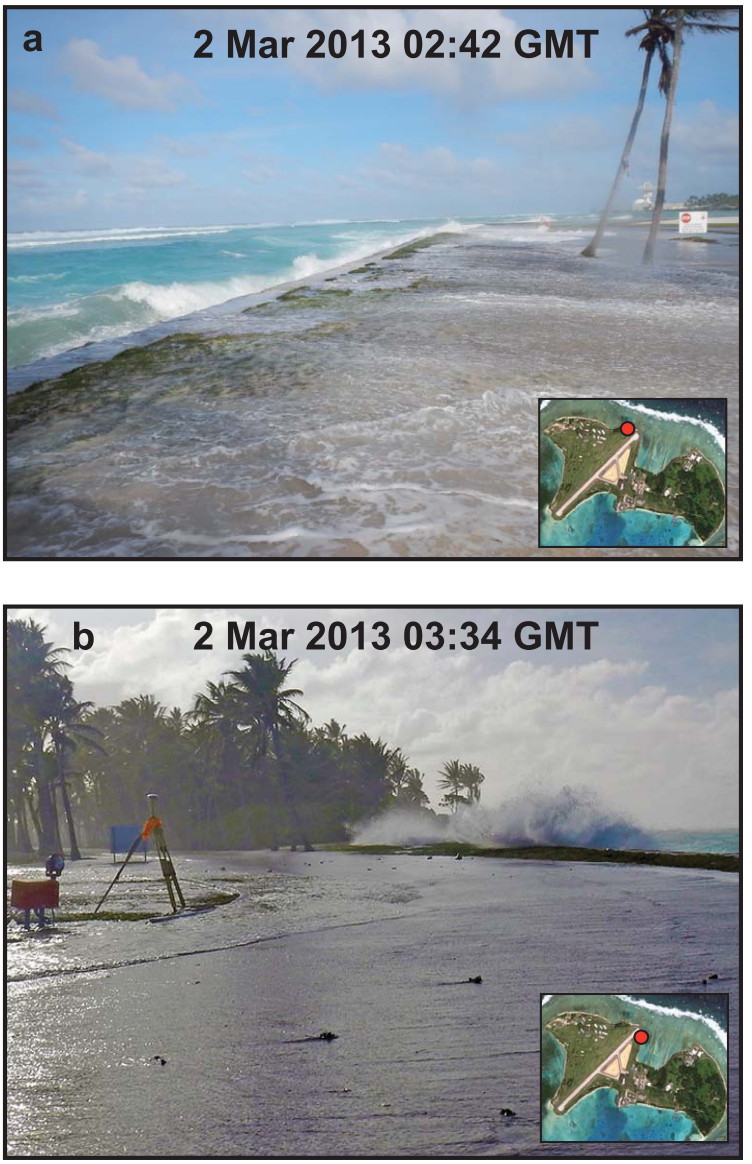

Figure 7. Two photographs taken during March 2014 large wave event that show the overwash and wave-driven flooding that occurred on the northwestern coastline of Roi-Namur. Inset maps show location of where each photo was taken.

Although both the December and March wave events produced overwash and flooding of the island, the flooding during the March event was more substantial. The RMI government declared a state of emergency following the March event, which not only caused flooding on Roi-Namur, but also considerable inundation and structural damage to other atoll islands across RMI, including contaminating water and agriculture reserves (see United National Office for the Coordination of Humanitarian Affairs, www.unocha.org). Eyewitness accounts (P. Swarzenski, personal communication, 2013) and photos taken on Roi-Namur (Figure 7) during the March event indicate instances of overwash occurring within a narrow window of time that coincided with the peak of a spring tide (Figure 6, shaded boxes). We will refer to this time window as the "overwash period", but emphasize that only instances of overwash were occurring (i.e., not continuous overwash). The overwash period was also when outer reef flat $H_{s,IG}$, inner reef flat $H_{s,IG}$, and maximum instantaneous water levels, h', reached peak levels of 2.8 m at the toe of the beach. We note that the photos and eyewitness account do not preclude the possibility of overwash also having occurred during the following high tide, which fell during early morning hours locally, before civil twilight. Notably, the documented period of overwash occurred before offshore wave heights peaked and did not coincide with maximum reef flat η. However, η over both reef flat transects was approximately 0.5 m during the observed overwash, which, while not at a maximum, did comprise a consequential portion (~18%) of total overall water levels. Still, the overwash window ended as the tidal stage dropped, even as offshore waves and η increased, indicating the importance of overall water levels for the ability of both short-period and long-period waves to propagate over the reef flat.

To produce the observed overwash, we presume that there were instances when the inner reef flat water levels (including η) combined with nearshore wave dynamics were capable of exceeding the vertical heights of the coastal berms (Figure 6). The maximum expected runup, R_{max}, can be estimated using the wave conditions measured at the inner reef flat sites. R_{max} was calculated after *Nwogu and Demirbilek* [2010], using the *Hunt* [1958] formulation $R_{\max} = H_{rms}\xi$, where ξ is the Iribarren number (or surf similarity

parameter), $\xi = \tan\beta / \sqrt{2\pi H_{rms}/gT_p^2}$, with $\tan\beta$ equal to the slope of the beach face (~1:6 for our sites). Using the wave parameters measured at the inner reef flat sites, an R_{max} was calculated separately for IC and the low-frequency waves. Here we did not find it appropriate to delineate the IG and VLF bands; the energy spectra exhibit a bimodal profile (Figure 2) and, as such, we chose to use a representative low-frequency T_p from the combined IG and VLF bands. This approach to runup, with the use of ξ, treats these reformed (i.e., shoreward of the reef crest) waves over the reef flat as in-coming waves approaching a planar beach face and does not take into account the wave breaking dynamics at the reef crest. Showing agreement with the reflection coefficient discussed in section 3.1, the corresponding ξ values for the low-frequency waves are large ($\xi > 1$), further indicating that these waves were predominantly reflected at the shoreline. Runup values for the IC and low-frequency waves were summed to give an approximate total runup, which is taken to represent the upper limit of possible vertical runup due to waves at the shoreline. The vertical height from the inner reef flat site to the highest point of the coastal berm was approximately 3.3 m for the NW transect and 3.8 m for the NE transect, as measured at the beginning of the deployment. Light Detection and Ranging (LIDAR) profiles taken at the end of the deployment showed very little change in the beach berm vertical heights (J. Logan, personal communication, 2014). During the observed overwash time window, the water level plus the total R_{max} exceeded the 3.3 m berm height at the NW inner reef flat, and was just below the 3.8 m berm height ($R_{max} = 3.7$ m) at the NE site (Figures 6o and 6p). The combined $h + R_{max}$ was also greater than the NW berm height during the December event, suggesting that overwash may have occurred on that part of the island during that event as well (Figure 5o). During both events, the contribution to R_{max} by low-frequency waves exceeded 80% at both sites, underscoring how reef flat low-frequency waves may act as the primary drivers of overwash at this site.

Merrifield et al. [2014] estimated extreme shoreline water levels on Roi-Namur using a summation of setup and the standard deviation of surface elevation over the IC and IG bands, and predicted that wave inundation would occur when this level exceeded 2.0 m. Applying this formulation to our data, we find extreme shoreline water levels of 1.9 m at both transects during the March event overwash period. The *Merrifield et al*. [2014] model hindcasts for the December 2008 large overwash event estimated total extreme water levels of 1.9 m during the high tides, matching our in situ measurements for the March 2014 event. Given the good agreement (i.e., within the uncertainty) with our measurements, the *Merrifield et al*. [2014] formulation seems applicable to this study site.

3.3. Anomalous Wave Runup Event

An anomalous wave runup event, serendipitously captured both by the oceanographic sensors and a shore-based time-lapse camera, provides another example of how offshore water levels coupled with low-frequency waves on the reef flat can produce extreme shoreline effects. On 18 November 2013 at 04:17:17 GMT, the NW alongshore-oriented camera imaged a large runup event (Figure 8a). Analysis of the photo, performed by *Quataert* [2015], estimated a maximum vertical runup height (which includes h and η) of 3.3 m at the time the photo was taken. Using the burst that coincided with the camera photo, our estimated total runup at the NW site gives an $h + R_{max} = 3.5$ m. We consider this significant runup event "anomalous" not only because it was the sole runup event captured in the camera time series, but because it did not occur during a large offshore wave event. Offshore wave conditions during the ±6 h around this event were moderate, with average $H_{off} = 2$ m and $T_p = 14$ s, with no large variations (Figure 3). However, it did coincide with the second-largest peak water level during a spring tide, with $h_{off} = 0.7$ m above the mean. At this tidal peak, the full-burst h' record shows a large (maximum height ~ 1.6 m) wave packet at the NW fore reef from approximately 04:16–04:17 (Figure 8c). The signature of this wave packet can be seen propagating across the reef flat (Figures 8d–8f). From the outer to the inner reef flat, the amplitude of the band-pass filtered h' peaks associated with this packet decreased by 0.5 m for the IC band, remained constant for the IG band, and increased 0.2 m for the VLF band. At 04:17:20—within a few seconds of the runup shown in the photo—the resulting inner reef flat instantaneous h'-h (i.e., above mean water level) reached just over 1.0 m (Figure 8f), corresponding to a total overall h' of 2.2 m. The relative contributions of the IC, IG, and VLF amplitudes to the peak h' were 31, 39, and 30%, respectively.

Taking the inner reef flat h' characteristics during the November anomalous event as a proxy for runup events not captured by the camera, we developed a runup event finder and applied it to the entire NW inner reef flat record. For each burst, this event finder looked at h' minus the burst mode and identified peaks > 0.9 m. The 0.9 m threshold was chosen based on the 18 November runup event. As expected, the

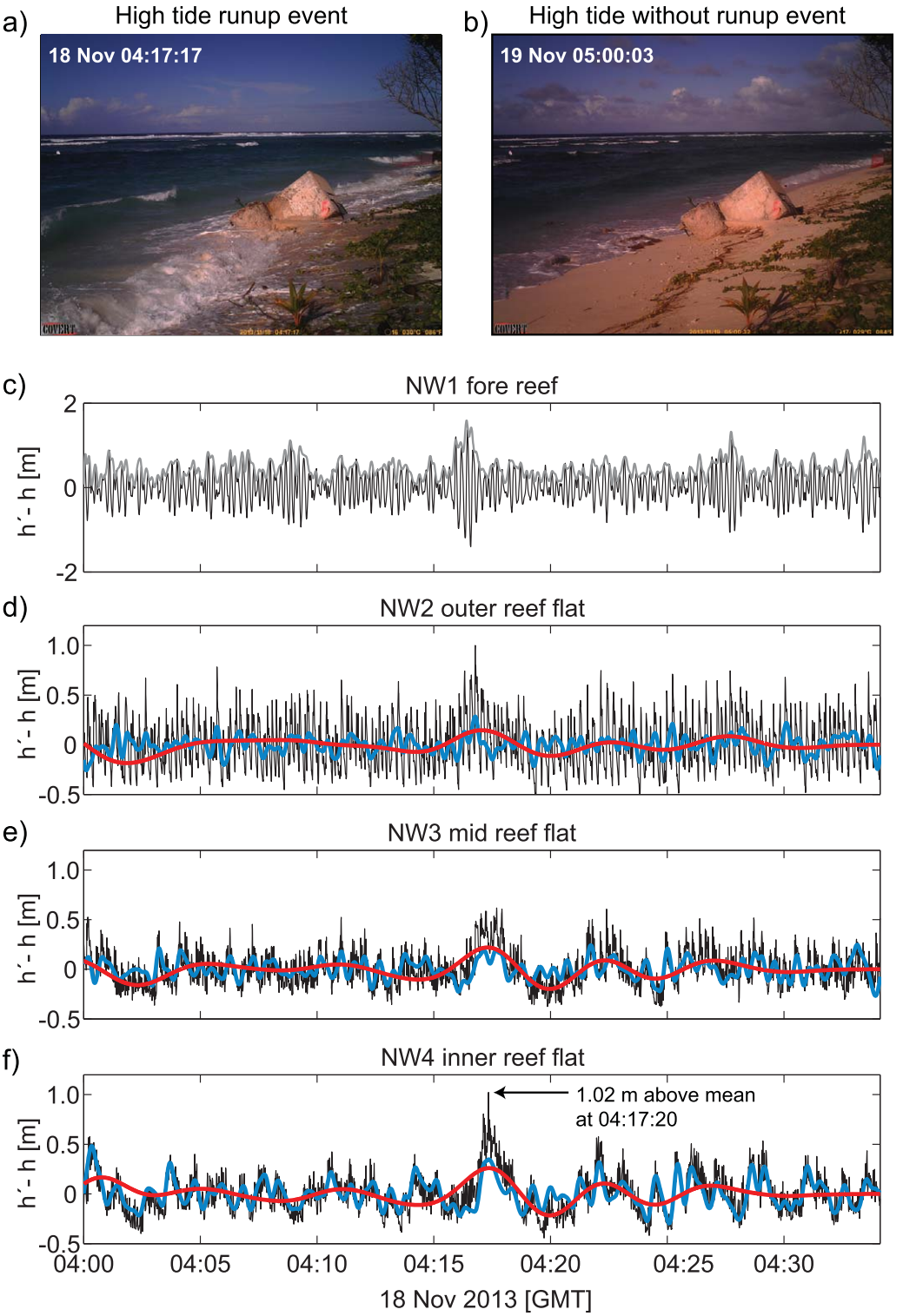

Figure 8. Details from an anomalous runup event captured in both the time-lapse camera and wave gauges of the NW transect. (a) Photograph taken of the runup event, which was estimated to have reached 3.3 m vertically up the beach face [*Quataert*, 2015]. (b) For comparison, a photo taken the next day at same tidal stage as Figure 8a but with no runup event. Instantaneous water level measurements above the burst mean from the (c) fore reef, (d) outer, (e) mid, and (f) inner reef flat. In Figure 8c, the wave envelope amplitude is also shown (gray line). Reef flat plots include the infragravity (blue) and very low frequency (red) band-pass filtered water level records. At the inner reef flat site, water levels of 1 m above the mean occurred at 04:17:20, within a few seconds of the photo in Figure 8a.

majority of these possible NW runup events occurred during higher tidal stages, with over 50% occurring when $h_{off} \geq 0.5$ m above the mean. Large beach runup events, as defined by our indicator, were also possible during low tides, however, larger fore reef waves were required. Approximately 11% of the runup events occurred when h_{off} was below mean water level, but all of these except one occurred during the December and March large wave events. The one exception happened on 20 February 2014, when mean H_{off} was 2.0 m, h_{off} was −0.2 m below the mean, and a large (2.5 m) wave packet was observed at the fore reef, which subsequently resulted in a total $h + h'$ peak of 1.4 m. The IC, IG, and VLF amplitudes associated with this peak were 0.2, 0.6, and 0.4 m, respectively. Consequently, extreme shoreline runup events are possible even under moderate offshore wave conditions, but are most likely during periods of high water levels. Model projections for Roi-Namur have also shown how high extreme water levels can occur with moderate offshore wave conditions when they coincide with peak spring tides [*Merrifield et al*., 2014]. Both the 18 November anomalous runup event and the possible one on 20 February demonstrate how offshore water levels and low-frequency reef flat waves can lead to large runup at the shoreline, which can occur in the absence of exceptionally large offshore waves.

4. Discussion

Over the Roi-Namur reef flat, low-frequency waves, together with offshore water levels, appear to be the primary drivers of extreme water level dynamics at the shoreline, in terms of their dominant role in runup and overwash—processes that affect shoreline morphology, erosion/accretion, and coastal flooding. The two large wave events we observed on Roi-Namur had wave heights that occur approximately every 1–2 years for the northern Marshall Islands [*Storlazzi et al*., 2015b], usually in the boreal winter months [*Merrifield et al*., 2014]. However, the frequency and severity of these wave events vary inter-annually according to El Niño-Southern Oscillation (ENSO) phases [*Australian Bureau of Meteorology and CSIRO*, 2014]. The large waves impacting this region are generally wind-waves forced by distant midlatitude storms. The overwash and coastline flooding caused by the cooccurrence of large waves and high tides are phenomena that are not unique to Roi-Namur Island, but have been observed at numerous Pacific islands and are a concern for the majority of populations living near fringing reef-lined coasts [*Hoeke et al*., 2013].

4.1. Reef Morphology and Low-Frequency Wave Propagation

The reef morphology on Roi-Namur may be particularly suited to support the propagation of IG and VLF waves. Similar to other relatively smooth, low-relief reef flats, the low-frequency waves we observed appear to undergo very little frictional dissipation and exhibited large increases in energy toward shore, particularly with raised water levels. Following *Lowe et al*. [2005] and *Péquignet et al*. [2011], we can estimate the wave friction factor, f_w, for the Roi-Namur reef using a formula relating f_w to bottom roughness:

$$f_w = \exp\left[a_1\left(\frac{r}{A}\right)^{a_2} + a_3\right] \tag{7}$$

where r is the bed roughness and A is the wave orbital diameter at the bed, given by $A = H_{rms}/\sinh(kh)$, with k being the wave number determined by the linear dispersion relationship for surface gravity waves, H_{rms} taken from the IC band. The a_1, a_2, and a_3 coefficients are empirically derived, and we used the values provided by *Nielson* [1992] for a fully developed, rough turbulent regime: $a_1 = 5.5$, $a_2 = 0.2$, and $a_3 = -6.3$. We used an $r = 0.14$ m from *Lowe et al*. [2005], an empirically derived estimate from a large barrier reef at Kaneohe, Hawaii, USA. Based on visual observations, this roughness length scale—equivalent to a rugosity on the order of tens of centimeter—seems reasonable for the Roi-Namur reef flat. Roughness scales of the same order of magnitude have been used for the Ipan, Guam, reef [*Péquignet et al*., 2011] and Ningaloo, Western Australia [*A. Pomeroy et al*., 2012a]. Taking the mean value across all three reef flat sites for each transect, a mean wave friction factor of $f_w = 0.11$ is estimated for the NE transect and $f_w = 0.09$ for the NW transect. These values agree with estimates for other similarly smooth, low-relief reefs, such as Ipan, Guam ($f_w \sim 0.12$ [*Péquignet et al*., 2011]), and John Brewer reef, Australia ($f_w = 0.08 - 0.22$ [*Nelson*, 1996]), and are lower than estimates from reefs with greater coral coverage and bathymetric complexity (e.g., $f_w = 0.28$ from *A. Pomeroy et al*. [2012a]).

4.2. Reef Flat Resonance

In addition to the relatively low bottom friction (for a reef environment), the narrow reef geometry may have led to excitation of resonant frequencies over the Roi-Namur reef flat, which would act to further

amplify the amount of energy at the shoreline, especially under storm conditions. Indeed, the elevated energy observed in the VLF band may be a by-product of this resonance. During tropical storm Man-Yi, the increased water level setup over the Ipan, Guam, reef flat enabled a resonant response that led to coastal wave-driven flooding [*Péquignet et al*., 2009]. This resonant forcing and VLF patterns over the Ipan reef were found to be caused by the modulation of breaking swell waves at the reef crest [*Péquignet et al*., 2009]. A subsequent modeling study based on the Ipan observations found that the forcing of resonant modes over this reef was dependent on not only the increase in water levels due to the storm event, but also the frictional characteristics of the reef flat; dissipation due to bottom friction counteracts the excitation of resonant frequencies by dampening the amplification peaks at the shoreline [*A. W. M. Pomeroy et al*., 2012b]. Thus, for a given reef geometry and water depth, one would expect smoother, lower relief reefs, such as Roi-Namur, to be subject to greater shoreline amplification due to resonance modes. The cross-reef wave energy profiles for the IG and VLF waves further suggest the establishment of standing modes over our study area (Figures 4e and 4i).

Theoretical reef flat resonance periods can be investigated using the open basin estimate [e.g., Chapman and Giese, 2009]:

$$T_n = \frac{4L}{(2n+1)\sqrt{gh}} \quad n = 0,\ 1,\ 2\ \ldots \tag{8}$$

where L is reef flat width and h is water depth. This can be applied to the NW and NE sections of the Roi-Namur reef flat, which have L of 270 and 344 m, respectively, and using h as the water level averaged across all three reef flat sensors. The fundamental resonance modes for the Roi-Namur reef range from 263 to 770 s for the NW transect, and 323 to 981 s for the NE transect; these ranges fall well within VLF band, even for very low water levels. For the n = 1 mode, resonance periods range from 132 to 533 s for the NW transect, and 164 to 809 s for the NE transect, indicating possible resonance at this higher mode within the IG band as well. Thus, in contrast to Ipan, Guam, the narrower Roi-Namur reef flat may be subject to resonance under a range of water levels, not just those during extreme storm conditions.

To test this further, three indicators used by *A. W. M. Pomeroy et al*. [2012b] to identify instances of resonance between the outer and inner reef flat sites can be applied: (1) high coherence ($>$0.9) between the two water level surface records, (2) a 0° or 180° phase difference, and (3) amplification of the signal at the inner reef flat site, defined as the ratio of the spectral energies at the inner to outer reef flat sites being $>$1. Furthermore, once all three criteria have been met, the identified resonant frequencies must match the theoretical modes (equation (8)) set by the water depth and reef flat geometry. Applying these indicators to each burst record, resonance was identified at the n = 0, 1, and 2 modes in 4%, 17%, and 15% of the NW bursts, respectively, for an overall resonance incidence throughout the entire study period of 36%. Resonance was found across a range of water levels, but was more likely to occur when water levels were greater than average; the mean $\pm$1 std. deviation of the overall reef flat water level at times of resonance was 0.90 $\pm$ 0.24 m, compared to the overall mean reef flat water level of 0.61 $\pm$ 0.32 m. The incidence of resonance was much lower at the NE transect, with 3%, 6%, and 6% of the bursts at the n = 0, 1, and 2 modes, respectively, passed the resonance criteria, for an overall resonance incidence of 15%. The greater incidence of resonance at the NW transect is likely due to the narrower reef flat width. Resonance at the NE transect was also more likely during higher water levels, with a mean reef flat water level during times of resonance of 1.05 $\pm$ 0.27 m, compared to 0.74 $\pm$ 0.34 m for the overall record.

During the March large wave event, the fraction of bursts with identified resonance in the first three modes increased to 44% for the NW transect and to 21% for the NE transect. Interestingly, the instance of resonance decreased slightly during the December event, to 35% for the NW transect and to 8% for the NE, most likely due to the smaller tidal range that occurred with the December event. We speculate that difference in resonance behavior may not only be due to the differing offshore water levels during the two wave events, but also the different angles of these shore-normal transects relative to the incoming waves (see section 3.2). The effects of coastline curvature and offshore wave direction on resultant low-frequency wave dynamics on reef flats are currently not well understood. In a modeling study applied to the Puerto Morelos fringing reef lagoon, *Torres-Freyermuth et al*. [2012] also found that nearshore low-frequency wave dynamics were highly sensitive to reef geometry, with IG wave energy and resonance increasing with decreasing reef width. Additionally, in their observations of overwash on the coast of Guam after Typhoon Russ, *Jaffe and*

Richmond [1992] noted an inverse relationship between reef flat width and overwash elevation on the adjacent coast. For the Roi-Namur reef flat, the low frictional characteristics, coupled with the narrow reef width, likely drive a high degree of resonance over the reef flat, causing amplification of water levels and low-frequency waves at the shoreline. The narrower portions of the reef appear to be more susceptible to these amplification dynamics, and, thus, the coastline near these areas might be more prone to overwash and flooding by extreme storm events.

4.3. Shoreline Accretion and Erosion

Taken together, the relative skewness and asymmetry of the low-frequency waves, coupled with reef flat resonance, may be an important mechanism of sediment transport over shallow reef flats. A laboratory experiment by *Pomeroy et al*. [2015] found that for smooth, shallow reef flats, the sediment transport at the back of the reef (i.e., closest to the shoreline) had a considerable contribution from low-frequency wave motions that resulted in shoreward transport. Similar to the shape of the IG waves we observed over the Roi-Namur reef flat, the low-frequency waves driving this transport had high positive skewness and negative asymmetry close to shore. In addition to the shape of the waveforms, standing wave patterns also have the potential to affect sediment transport patterns over reef flat, as has been reported for planar beach environments. The location and movement of sandbars has been linked to standing wave patterns, with accumulation of seafloor material associated with the nodes and antinodes of standing low-frequency waves [e.g., *Short*, 1975; *Holman and Bowen*, 1984; *Aagaard et al*., 1994]. In addition, these low-frequency standing waves may differentially transport different grain sizes, effectively sorting coarser sands from fine-grain material [*Landry et al*., 2007]. It is currently unclear how standing-wave behavior affects transport of sediment over reef flats. However, it is probable that the shoreline accretion and erosion patterns along fringing reef-lined coasts are affected by not only the skewness and asymmetry of these low-frequency waves but also resonance dynamics over the reef flat. Given the highly energetic, skewed, asymmetrical IG waves observed during the large wave events on Roi-Namur, these effects on sediment transport are likely most pronounced during such energetic events. And, as a consequence, large wave events impacting the seaward shoreline of a fringing reef-lined coast may act as island accretionary events [*Maragos et al*., 1973; *Woodroffe*, 2008; *Webb and Kench*, 2010; *Smithers and Hoeke*, 2015].

4.4. Low-Frequency Waves and Subsequent Shoreline Runup

It is becoming clear that an accurate assessment of how waves and water levels affect fringing-reef coasts must also consider shoreline runup. As emphasized by *Beetham et al*. [2015], in terms of temporal exposure, runup is the primary process connecting reef flat water dynamics and the beach face. Laboratory and modeling studies have demonstrated how low-frequency waves over reef flats are important drivers of runup on the adjacent shorelines [*Seelig*, 1983; *Nwogu and Demirbilek*, 2010; *Beetham et al*., 2015; *Shimozono et al*., 2015]. Our long-term in situ measurements from Roi-Namur corroborate this further; during both the large wave events and the anomalous runup event, low-frequency waves, particularly in the IG band, made the dominant contribution to overall runup, and this runup was largest during the highest water levels. Recent modeling studies indicate that runup along fringing reef-lined coasts is expected to increase under rising sea levels, particularly for coastlines fronted by relatively narrow (widths < 300 m) reef flats [*Beetham et al*., 2015; *Quataert et al*., 2015; *Shimozono et al*., 2015]. In addition, if rising water levels lead to increased excitation of resonance frequencies, this could further amplify shoreline runup [*Nwogu and Demirbilek*, 2010; *Shimozono et al*., 2015].

4.5. Climate Change and Coastal Hazards for Fringing Reef-Lined Coasts

There is increasing interest in how coastal hazards will evolve with current climate and sea level rise projections, and, recently, there has been focus on fringing coral reef coastlines, which appear to be particularly at risk to changing global conditions [e.g., *Nicholls et al*., 2007]. Sea level is expected to rise 0.4–1.8 m by year 2100 [*Kopp et al*., 2014], and the rate of increase may be accelerating for the western tropical Pacific [*Merrifield*, 2011]. Because vertical reef flat accretion rates in high-energy areas (1–4 mm yr^{-1}) [*Montaggioni*, 2005] are up to an order of magnitude smaller than the rates of projected sea level rise [*Kopp et al*., 2014], projected sea level rise will outstrip new reef flat accretion, resulting in net increase in water depth over coral reef flats. Higher water levels over reef flats would leave these shorelines more vulnerable to large waves.

Model projections of the how the storm and wind-wave climate in the equatorial Pacific will change over the next century are inconclusive, and the predicted trends have a high degree of uncertainty [*Mori et al*., 2010; *Young et al*., 2011; *Dobrynin et al*., 2012; *Fan et al*., 2013; *Hemer et al*., 2013; *Australian Bureau of Meteorology and CSIRO*, 2014; *Storlazzi et al*., 2015b]. However, even with a reduction in significant wave heights and/or the frequency of tropical cyclones, rising water levels will increase the ability of offshore waves to transmit energy across reef flats to the shoreline [*Storlazzi et al*., 2011; *Becker et al*., 2014; *Taebi and Pattiaratchi*, 2014; *Hoeke et al*., 2013]. Therefore, with sea level rise, future overwash and flooding events may transpire with smaller waves.

In addition to changes in atmospheric and oceanographic forcing, coral degradation caused by increasing sea temperatures [*Hoegh-Guldberg*, 1999] and ocean acidification [*Pandolfi et al*., 2011] could further increase the vulnerability of these coasts to wave impacts by decreasing the frictional dissipation of waves [*Sheppard et al*., 2005; *Quataert et al*., 2015]. For reefs with higher coral coverage, damage to coral communities through climate change effects will likely result in not only increased transmission of wave energy over the reef flat, but also a shift of this energy to lower frequencies, leading to greater dominance of longer-period waves on the reef flat [*Ma et al*., 2014].

Thus, while it remains unclear how the wave climatology of the equatorial Pacific will change over the next century, based on potential sea level rise and coral degradation, we predict (1) that overwash events will be possible with less extreme offshore wave heights, and (2) an increase in the transfer of wave energy from the offshore incident to the low-frequency band over the reef flat. These potential outcomes point to an overall intensification of the wave power impacting the shorelines along fringing reef-lined coasts as well as the increased vulnerability of these coasts to wave-driven coastal hazards [e.g., *Storlazzi et al*., 2015a].

5. Conclusions

The recent focus on reef flat hydrodynamics by a number of field-based, model-based, and laboratory-based studies has greatly improved our understanding of how the energy associated with offshore processes transforms and transmits across reef flats to impact fringing reef-lined coasts. This growing body of work points to the dominant role of low-frequency waves and resonance over these reef flats, particularly at the shoreline. With our 5 month field study of wave dynamics and wave-driven water levels on a fringing coral reef on Roi-Namur Island, RMI, we present direct in situ observations of reef flat waves across a range of water level and offshore conditions, including two large wave events that had maximum wave heights greater than 6 m with peak periods of 16 s over the fore reef. Low-frequency waves were found to be the primary contributors to not only overwash during large offshore wave events, but also runup. During the larger event, which coincided with a peak spring tide, infragravity (IG; 0.04–0.004 Hz) and very low frequency (VLF; 0.004–0.001 Hz) wave heights of 1.0 and 0.7 m, respectively, were observed at the shoreline. During this event, instances of overwash were observed for a 3 h period, which coincided with high tide and the largest low-frequency reef flat wave heights. These low-frequency waves were the major contributors to runup at the shoreline. This runup, combined with the elevated water surface elevations, reached 3.7 m above the toe of the beach at the inner edge of the reef flat, exceeding the vertical height of the beach berm. The IG waves were also highly skewed and asymmetrical, but due to the steep beach face, were most likely in a fully reflective regime.

The narrow reef width and low frictional characteristics of the Roi-Namur study site likely further enhanced low-frequency wave propagation and resonance on the reef flat. Throughout the study, both the IG and VLF wave energies exhibited resonance patterns, particularly across the narrower reef flat, and this resonance occurred more frequently with higher reef flat water levels. The combination of the skewed, asymmetrical IG waves and reef flat resonance observed during the large wave events suggests that these low-frequency motions may disproportionally drive sediment transport over the reef and at the shoreline during these high energy events. However, more research is needed to investigate how these irregular waveforms interact with standing wave patterns.

One of the motivating factors behind the recent research on fringing coral reef coastlines is concern over how climate change and sea level rise may adversely affect the communities and resources associated with these coastal areas. With the projected change in global conditions, we expect to see higher water levels and a decrease in the frictional characteristics of these reefs. Consequently, these fringing reef flat

environments may become increasingly dominated by low-frequency wave dynamics. Our results demonstrate how these changes will likely result in more frequent and higher-impact overwash and runup events. Therefore, in order to use global and regional wave models to accurately characterize extreme shoreline water levels and coastal hazards for fringing reef coastlines, it is critical to take into account how offshore conditions and reef flat morphology drive inner reef flat wave dynamics, particularly in the low-frequency spectrum.

Acknowledgments

This work was funded by U.S. Department of Defense's Strategic Environmental Research and Development Program (SERDP) under project RC-2334 and the U.S. Geological Survey's Coastal and Marine Geology Program. We thank T. Reiss, J. Logan, and P. Swarzenski (USGS), as well as G. Piniak and D. Field (NOAA) for their help with instrument deployment and data collection. We thank E. Quataert, A. van Dongeren, and M. Gawehn (Deltares) for helpful collaborations. We also thank the Captain and crew of the *D/V Patriot*, D. Miller and C. Nakasone (Kwajalein Range Services), and the U.S. Army Garrison-Kwajalein Atoll (USAG-KA) for their support of this project. We are grateful to A. Pomeroy (UWA) for helpful discussions, J. Lacy (USGS) for an initial review of the manuscript, and two anonymous reviewers for their thoughtful and constructive comments. Data used in this study are available upon request to the corresponding author (ocheriton@usgs.gov). Use of trademark names does not imply USGS endorsement of products.

References

Aagaard, T., and B. Greenwood (1995), Suspended sediment transport and morphological response on a dissipative beach, *Cont. Shelf Res.*, *15*, 1061–1086, doi:10.1016/0278-4343(94)00068-X.

Aagaard, T., N. Nielsen, and J. Nielsen (1994), Cross-shore structure of infragravity standing wave motion and morphological adjustment: An example from Northern Zealand, Denmark, *J. Coastal Res.*, *10*(3), 716–731.

Australian Bureau of Meteorology and CSIRO (2014), Climate variability, extremes and change in the Western Tropical Pacific: New science and updated country reports, Pacific-Australia Climate Change Science and Adaptation Planning Program technical report, Aust. Bur. of Meteorol. and Commonw. Sci. and Ind. Res. Organ., Melbourne, Victoria, Australia.

Battjes, J. A. (1974), Surf similarity, *Coast. Eng. Proc.*, *1*(14), 466–480, doi:10.9753/icce.v14.

Becker, J. M., M. A. Merrifield, and M. Ford (2014), Water level effects on breaking wave setup for Pacific Island fringing reefs, *J. Geophys. Res. Oceans*, *119*, 914–932, doi:10.1002/2013JC009373.

Beetham, E., P. S. Kench, J. O'Callaghan, and S. Popinet (2015), Wave transformation and shoreline water level on Funafuti Atoll, Tuvalu, *J. Geophys. Res. Oceans*, *121*, 311–326, doi:10.1002/2015JC011246.

Brander, R. W., P. S. Kench, and D. Hart (2004), Spatial and temporal variations in wave characteristics across a reef platform, Warraber Island, Torres Strait, Australia, *Mar. Geol.*, *207*, 169–184, doi:10.1016/j.margeo.2004.03.014.

Chapman, D. C., and G. S. Giese (2009), Seiches, in *Elements of Physical Oceanography*, edited by J. H. Steele et al., pp. 55–61, Academic, Waltham, Mass.

Dean, R. G., and R. A. Dalrymple (1991), *Water Wave Mechanics for Engineers and Scientists*, vol. 2, World Sci., Hackensack, N. J.

de Bakker, A. T. M., M. F. S. Tissier, and B. G. Ruessink (2014), Shoreline dissipation of infragravity waves, *Cont. Shelf Res.*, *72*, 73–82, doi:10.1016/j.csr.2013.11.013.

Dobrynin, M., J. Murawsky, and S. Yang (2012), Evolution of the global wind wave climate in CMIP5 experiments, *Geophys. Res. Lett.*, *39*, L18606, doi:10.1029/2012GL052843.

Fan, Y., I. M. Held, S-J. Lin, and X. L. Wang (2013), Ocean warming effect on surface gravity wave climate change for the end of the Twenty-First Century, *J. Clim.*, *26*, 6046–6066, doi:10.1175/JCLI-D-12-00410.1.

Ferrario, F., M. W. Beck, C. D. Storlazzi, F. Micheli, C. C. Shepard, and L. Airoldi (2014), The effectiveness of coral reefs for coastal hazard risk reduction and adaptation, *Nat. Commun.*, *5*, 3794, doi:10.1038/ncomms4794.

Ford, M. R., J. M. Becker, and M. A. Merrifield (2013), Reef flat wave processes and excavation pits: Observations and implications for Majuro Atoll, Marshall Islands, *J. Coastal Res.*, *29*(3), 545–554, doi:10.2112/JCOASTRES-D-12-00097.1.

Grady, A. E., L. J. Moore, C. D. Storlazzi, E. Elias, and M. A. Reidenbach (2013), The influence of sea level rise and changes in fringing reef morphology on gradients in alongshore sediment transport, *Geophys. Res. Lett.*, *40*, 3096–3101, doi:10.1002/grl.50577.

Grasso, F., H. Michallet, and E. Barthélemy (2011), Sediment transport associated with morphological beach changes forced by irregular asymmetric, skewed waves, *J. Geophys. Res.*, *116*, C03020, doi:10.1029/2010JC006550.

Hardy, T. A., and I. R. Young (1996), Field study of wave attenuation on an offshore coral reef, *J. Geophys. Res.*, *101*(C6), 14,311–14,326, doi:10.1029/96JC00202.

Hemer, M. A., Y. Fan, N. Mori, A. Semedo, and X. L. Wang (2013), Projected changes in wave climate from a multi-model ensemble, *Nat. Clim. Change*, *3*, 471–476, doi:10.1038/nclimate1791.

Hench, J. L., J. J. Leichter, and S. G. Monismith (2008), Episodic circulation and exchange in a wave-driven coral reef and lagoon system, *Limnol. Oceanogr.*, *53*, 2681–2694, doi:10.4319/lo.2008.53.6.2681.

Hoegh-Guldberg, O. (1999), Climate change, coral bleaching and the future of the world's coral reefs, *Mar. Freshwater Res.*, *50*, 839–866, doi:10.1071/MF99078.

Hoeke, R. K., K. L. McInnes, J. C. Kruger, R. J. McNaught, J. R. Hunter, and S. G. Smithers (2013), Widespread inundation of Pacific islands triggered by distance-source wind-waves, *Global Planet. Change*, *108*, 128–138, doi:10.1016/j.gloplacha.2013.06.006.

Holman, R. A., and A. J. Bowen (1984), Longshore structure of infragravity wave motions, *J. Geophys. Res.*, *89*(C4), 6446–6452, doi:10.1029/JC089iC04p06446.

Hunt, I. A. (1958), *Design of Seawalls and Breakwaters*, U.S. Lake Surv., U.S. Army Corps of Eng., Detroit, Mich.

Jaffe, B. E., and B. M. Richmond (1992), Overwash variability on the shoreline of Guam during Typhoon Russ, in *Proceedings of 7th International Coral Reef Symposium*, vol. 1, pp. 257–264, University of Guam Press, UOG Station, Guam.

Kirby, J. T., and R. A. Dalrymple (1984), Verification of a parabolic equation for propagation of weakly-nonlinear waves, *Coastal Eng.*, *8*, 219–232, doi:10.1016/0378-3839(84)90002-4.

Kopp, R. E., R. M. Horton, C. M. Little, J. X. Mitrovica, M. Oppenheimer, D. J. Rasmussen, B. H. Strauss, and C. Tebaldi (2014), Probabilistic 21st and 22nd century sea-level projections at a global network of tide-gauge sites, *Earth's Future*, *2*, 383–406, doi:10.1002/2014EF000239.

Kunkel, C. M., R. W. Hallberg, and M. Oppenheimer (2006), Coral reefs reduce tsunami impact in model simulations, *Geophys. Res. Lett.*, *33*, L23612, doi:10.1029/20006GL027892.

Landry, B. J., M. J. Hancock, and C. C. Mei (2007), Note on sediment sorting in a sandy bed under standing water waves, *Coastal Eng.*, *54*, 694–699, doi:10.1016/j.coastaleng.2007.02.003.

Lee, T. T., and K. P. Black (1978), The energy spectra of surf waves on a coral reef, in *Proceedings of 16th International Conference on Coastal Engineering*, pp. 588–608, Am. Soc. of Civ. Eng., Hamburg.

List, J. H. (1991), Wave groupiness variations in the nearshore, *Coastal Eng.*, *15*, 475–496, doi:10.1016/0378-3839(91)90024-B.

Longuet-Higgins, M. S., and R. W. Stewart (1960), Changes in the form of short gravity waves on long waves and tidal currents, *J. Fluid Mech.*, *8*, 565–583, doi:10.1017/S0022112060000803.

Longuet-Higgins, M. S., and R. W. Stewart (1962), Radiation stress and mass transport in gravity waves, with application to 'surf beats', *J. Fluid Mech.*, *13*, 481–504, doi:10.1017/S0022112062000877.

Longuet-Higgins, M. S., and R. W. Stewart (1964), Radiation stresses in water waves: A physical discussion, with applications, *Deep Sea Res. Oceanogr. Abstr.*, *11*, 529–562, doi:10.1016/0011-7471(64)90001-4.
Lowe, R. J., J. L. Falter, M. D. Bandet, G. Pawlak, M. J. Atkinson, S. G. Monismith, and J. R. Koseff (2005), Spectral wave dissipation over a barrier reef, *J. Geophys. Res.*, *110*, C04001, doi:10.1029/2004JC002711.
Lugo-Fernandez, A., H. H. Roberts, W. J. Wiseman Jr., and B. L. Carter (1998), Water level and currents of tidal and infragravity periods at Tague Reef, St. Croix (USVI), *Coral Reefs*, *17*, 343–349, doi:10.1007/s003380050137.
Ma, G., S.-F. Su, S. Liu, and J.-C. Chu (2014), Numerical simulation of infragravity waves in fringing reefs using a shock-capturing non-hydrostatic model, *Ocean Eng.*, *85*, 54–64, doi:10.1016/j.oceaneng.2014.04.030.
Malarkey, J., and A. G. Davies (2012), Free-stream velocity descriptions under waves with skewness and asymmetry, *Coastal Eng.*, *68*, 78–95, doi:10.1016/j.coastaleng.2012.04.009.
Maragos, J. E., G. B. K. Baines, and P. J. Beveridge (1973), Tropical cyclone Bebe creates a new land formation on Funafuti Atoll, *Science*, *181*, 1161–1164, doi:10.1126/science.181.4105.1161.
Merrifield, M. A. (2011), A shift in western tropical Pacific sea level trends during the 1990s, *J. Clim.*, *24*, 4126–4138, doi:10.1175/2011JCLI3932.1.
Merrifield, M. A., J. M. Becker, M. Ford, and Y. Yao (2014), Observations and estimates of wave-driven water level extremes at the Marshall Islands, *Geophys. Res. Lett.*, *41*, 7245–7253, doi:10.1002/2014GL061005.
Montaggioni, L. F. (2005), History of Indo-Pacific coral reef systems since the last glaciation: Development patterns and controlling factors, *Earth Sci. Rev.*, *71*, 1–75, doi:10.1016/j.earscirev.2005.01.002.
Mori, N., T. Yasuda, H. Mase, T. Tom, and Y. Oku (2010), Projection of extreme wave climate change under global warming, *Hydrol. Res. Lett.*, *4*, 15–19, doi:10.3178/HRL.4.15.
Nelson, R. C. (1996), Hydraulic roughness of coral reef platforms, *Appl. Ocean Res.*, *18*, 265–274, doi:10.1016/S0141-1187(97)00006-0.
Nicholls, R. J., P. P. Wong, V. R. Burkett, J. O. Codignotto, J. E. Hay, R. F. McLean, S. Ragoonaden, and C. D. Woodroffe (2007), Coastal systems and low-lying areas, in *Climate Change 2007: Impacts, Adaptation and Vulnerability, Contribution of Working Group II to the Fourth Annual Assessment Report of the Intergovernmental Panel on Climate Change*, edited by M. L. Parry et al., pp. 315–356, Cambridge Univ. Press, Cambridge, U. K.
Nielsen, P. (1992), Coastal bottom boundary layers and sediment transport, *Adv. Ser. Ocean Eng.*, vol. 4, World Sci., Hackensack, N. J.
Nwogu, O., and Z. Demirbilek (2010), Infragravity wave motions and runup over shallow fringing reefs, *J. Waterw. Port Coastal Ocean Eng.*, *136*, 295–305, doi:10.1061/(ASCE)WW.1943-5460.0000050.
Osborne, A. R., L. Bergamasco, M. Serio, L. Bianco, L. Cavaleri, M. Drago, L. Iovenitti, and D. Viezzoli (1996), Nonlinear shoaling of shallow water waves: Perspective in terms of the inverse scattering transform, *Il Nuovo Cimento C*, *19*, 151–176, doi:10.1007/BF02511838.
Pandolfi, J. M., S. R. Connolly, D. J. Marshall, and A. L. Cohen (2011), Projecting coral reef futures under global warming and ocean acidification, *Science*, *333*(6041), 418–422, doi:10.1126/science.1204794.
Peng, Z., Q. Zou, D. Reeve, and B. Wang (2009), Parameterisation and transformation of wave asymmetries over a low-crested breakwater, *Coastal Eng.*, *56*, 1123–1132, doi:10.1016/j.coastaleng.2009.08.005.
Péquignet, A.-C. N., J. M. Becker, M. A. Merrifield, and J. Aucan (2009), Forcing of resonant modes on a fringing reef during tropical storm Man-Yi, *Geophys. Res. Lett.*, *36*, L03607, doi:10.1029/2008GL036259.
Péquignet, A.-C. N., J. M. Becker, M. A. Merrifield, and S. J. Boc (2011), The dissipation of wind wave energy across a fringing reef at Ipan, Guam, *Coral Reefs*, *30*, 71–82, doi:10.1007/s00338-011-0719-5.
Péquignet, A.-C. N., J. M. Becker, and M. A. Merrifield (2014), Energy transfer between wind waves and low-frequency oscillations on a fringing reef, Ipan, Guam, *J. Geophys. Res. Oceans*, *119*, 6709–6724, doi:10.1002/2014JC010179.
Pomeroy, A., R. Lowe, G. Symonds, A. Van Dongeren, and C. Moore (2012a), The dynamics of infragravity wave transformation over a fringing reef, *J. Geophys. Res. Oceans*, *117*, C11022, doi:10.1029/2012JC008310.
Pomeroy, A. W. M., A. van Dongeren, R. J. Lowe, J. S. M. van Thiel de Vries, and J. Rovelvink (2012b), Low frequency wave resonance in fringing reef environments, *Coastal Eng. Proc.*, *1*(33), 1595–1604, doi:10.9753/icce.v33.currents.25.
Pomeroy, A. W. M., R. J. Lowe, A. R. van Dongeren, M. Ghisalberti, W. Bodde, and D. Roelvink (2015), Spectral wave-driven sediment transport across a fringing reef, *Coastal Eng.*, *98*, 78–94, doi:10.1016/j.coastaleng.2015.01.005.
Quataert, E. (2015), Wave runup on atoll reefs, MS thesis, Delft Univ. of Technol., Delft, Netherlands.
Quataert, E., C. Storlazzi, A. van Rooijen, O. Cheriton, and A. van Dongeren (2015), The influence of coral reefs and climate change on wave-driven flooding of tropical coastlines, *Geophys. Res. Lett.*, *42*, 6407–6415, doi:10.1002/2015GL064861.
Seelig, W. N. (1983), Laboratory study of reef-lagoon system hydraulics, *J. Waterw. Port Coastal Ocean Eng.*, *109*(4), 380–391, doi:10.1061/(ASCE)0733-950X(1983)109:4(380).
Sheppard, C., D. Dixon, M. Gourlay, A. Sheppard, and R. Payet (2005), Coral mortality increases wave energy reaching shores protected by reef flats: Examples from the Seychelles, *Estuarine Coastal. Shelf Sci.*, *64*(2–3), 223–234, doi:10.1016/j.ecss.2005.02.016.
Shimozono, T., Y. Tajima, A. B. Kennedy, H. Nobuoka, J. Sasaki, and S. Sato (2015), Combined infragravity wave and sea-swell runup over fringing reefs by super typhoon Haiyan, *J. Geophys. Res. Oceans*, *120*, 4463–4486, doi:10.1002/2015JC010760.
Short, A. D. (1975), Multiple offshore bars and standing waves, *J. Geophys. Res.*, *80*(27), 3838–3840, doi:10.1029/JC080i027p03838.
Smithers, S. G., and R. K. Hoeke (2015), Geomorphological impacts of high-latitude storm waves on low-latitude reef islands—Observations of the December 2008 event on Nukutoa, Takuu, Papua New Guinea, *Geomorphology*, *222*, 106–121, doi:10.1016/j.geomorph.2014.03.042.
Storlazzi, C. D., E. Elias, M. E. Field, and M. K. Presto (2011), Numerical modeling of the impact of sea-level rise on fringing coral reef hydrodynamics and sediment transport, *Coral Reefs*, *30*(1), 23–38, doi:10.1007/s00338-010-0705-3.
Storlazzi, C. D., E. P. L. Elias, and P. Berkowitz (2015a), Many atolls may be uninhabitable within decades due to climate change, *Sci. Rep.*, *5*, 14546, doi:10.1038/srep14546.
Storlazzi, C. D., J. B. Shope, L. H. Erikson, C. A. Hegermiller, and P. L. Barnard (2015b), Future wave and wind projections for United States and United States-affiliated Pacific Islands, *U.S. Geol. Surv. Open File Rep.*, *2015-1001*, 426 pp., doi:10.3133/ofr20151001.
Symonds, G., D. A. Huntley, and A. J. Bowen (1982), Two-dimensional surf beat: Long wave generation by a time-varying breakpoint, *J. Geophys. Res.*, *87*(C1), 492–498, doi:10.1029/JC087iC01p00492.
Taebi, S., and C. Pattiaratchi (2014), Hydrodynamic response of a fringing coral reef to a rise in mean sea level, *Ocean Dyn.*, *64*, 975–987, doi:10.1007/s10236-014-0734-5.
Terry, J. P., A. Y. A. Lau, and A. Etienne (2013), *Reef-Platform Coral Boulders: Evidence for High-Energy Marine Inundation Events on Tropical Coastlines*, Springer, Singapore, doi:10.1007/978-981-4451-33-8.
Torres-Freyermuth, A., I. Mariño-Tapia, C. Coronado, G. Medellin, A. Pedrozo-Acuña, R. Silva, J. Candela, and R. Iglesias-Prieto (2012), Modeling water levels in Puerto Morelos reef lagoon, *Nat. Hazards Earth Syst. Sci.*, *12*, 3765–3773, doi:10.5194/nhess-12-3765-2012.

Ursell, F. (1953), The long-wave paradox in the theory of gravity waves, *Proc. Cambridge Philos. Soc.*, *49*(4), 685–694.
U.S. Department of Interior (2006), *United States of American Insular Areas Energy Assessment Report*, Pac. Power Assoc., Suva. [Available at www.doi.gov/oia/reports/upload/U-S-Insular-Area-Energy-Assessment-Report-2006.pdf.]
van Dongeren, A., J. Battjes, T. Janssen, J. van Noorloos, K. Steenhauer, G. Steenbergen, and A. Reniers (2007), Shoaling and shoreline dissipation of low-frequency waves, *J. Geophys. Res.*, *112*, C02011, doi:10.1029/2006JC003701.
van Dongeren, A., R. Lowe, A. Pomeroy, D. M. Trang, D. Roelvink, G. Symonds, and R. Ranasinghe (2013), Numerical modeling of low-frequency wave dynamics over a fringing coral reef, *Coastal Eng.*, *73*, 178–190, doi:10.1016/j.coastaleng.2012.11.004.
Vetter, O., J. M. Becker, M. A. Merrifield, A.-C. Péquignet, J. Aucan, S. J. Boc, and C. E. Pollock (2010), Wave setup over a Pacific Island fringing reef, *J. Geophys. Res.*, *115*, C12066, doi:10.1029/2010JC006455.
Webb, A. P., and P. S. Kench (2010), The dynamic response of reef islands to sea-level rise: Evidence from multi-decadal analysis of island change in the Central Pacific, *Global Planet. Change*, *72*, 234–246, doi:10.1016/j.gloplacha.2010.05.003.
Woodroffe, C. D. (2008), Reef-island topography and the vulnerability of atolls to sea-level rise, *Global Planet. Change*, *62*, 77–96, doi:10.1016/j.gloplacha.2007.11.001.
Young, I. R. (1989), Wave transformations on coral reefs, *J. Geophys. Res.*, *94*(C7), 9779–9789, doi:10.1029/JC094iC07p09779.
Young, I. R., S. Zieger, and A. V. Babanin (2011), Global trends in wind speed and wave height, *Science*, *332*, 451–455, doi:10.1126/science.1197219.